# APPLICATION OF A WEIBULL STRESS MODEL TO PREDICT THE FAILURE OF SURFACE AND EMBEDDED CRACKS IN LARGE SCALE BEAMS MADE OF CLAD AND UNCLAD RPV STEEL

Shengjun Yin, Richard Bass, Paul Williams,
Oak Ridge National Laboratory, USA

Michael Ludwig, Elisabeth Keim,
Framatome ANP GmbH,
Freyeslebenstrasse 1, 91058 Erlangen, Germany;
e.mail:michael.ludwig@framatome-anp.com

## ABSTRACT

Within the European Network NESC, the project NESC IV deals with constraint effects of cracks in large scale beam specimens, loaded by uni- or biaxial bending moments and containing surface or embedded cracks. The specimens are fabricated from original US RPV material, being cladded or cladding is removed. All large scale tests have been conducted at ORNL outside the NESCIV project.

The outcome and the analyses of these uncladded and cladded beams containing the surface or embedded cracks are shown. By means of the finite element method, local approach methods and the Weibull stress models the specimens are analysed at the test temperatures and the probability of failure is calculated, taking into account constraint effects.

For the case of the embedded cracks it turned out that the failure moment of the uncladded beam is 5% lower than the one of the cladded beam. Both crack fronts of the embedded crack are supposed to fail at the same failure moment. The results of the analysis of the cladded beam showed that the upper crack front nearer to the surface fails prior to the lower crack front, which is located deeper in the specimen (the failure moment is 5% lower).

The numerical results agree very well with the experiments. The experimental failure moments could be well predicted and the failure scenario (which crack front fails first) could be determined. A theoretical shift in the transition temperature $T_0$ due to constraint effects could be defined for both crack fronts.

## INTRODUCTION

Several uniaxial and biaxial loaded large scale beam specimens with through-wall embedded and with surface cracks were tested at ORNL [2]. The specimens were fabricated from original RPV material, whereas two cladded and two uncladded specimens were investigated for the embedded cracks and seven specimens containing surface cracks. The experimental work is summarized in [1].

The results of the numerical studies conducted at ORNL and Framatome are summarized. Based on three-dimensional finite element calculations and Weibull calibration models both specimen types were calculated and failure moments are predicted. Constraint issues are investigated by means of the Weibull stress model.

## EXPERIMENTS

The special cruciform large scale bending specimens were developed during the HSST program to simulate the 3D loading conditions in the beltline region of an RPV subjected to pressurized thermal shock. The beams used for the investigation of surface and embedded crack effects are fabricated from the PVRUF material, where the material is taken from the longitudinal weld (surface cracks) and the plate base material (embedded cracks), [7].

The following data sets are considered:

| Material | Load Ratio | Defect dimensions | To (a/W=0.5, B=25) | No. of Tests |
|---|---|---|---|---|
| PVRUF weld [1] | Weld + Clad | Semi-elliptical 19x53 mm | -88.3 | 7 |
| PVRUF plate [1] | 0:1 | Embedded Slot 100x21 mm, 12 mm below surfce | -96.7 | 2 clad 2 unclad |

### Embedded cracks

The embedded crack specimens were fabricated by JRC/Petten/Netherlands, using Pressure Vessel Research User Facility (PVRUF) source material removed from reactor pressure vessel (RPV) shell segments available from a pressurized-water RPV that was never in service. All embedded crack beams were tested at ORNL to failure in cleavage under uniaxial loading. In Fig. 1 different steps for fabrication of the beams are shown: the cladded insert taken from the RPV shell with the embedded crack in a distance of 5 mm from the cladding to base material interface and the insert with the beam arms welded afterwards. The fabrication of the beams without

cladding is identical, but the cladding is removed before insertion of the embedded crack.

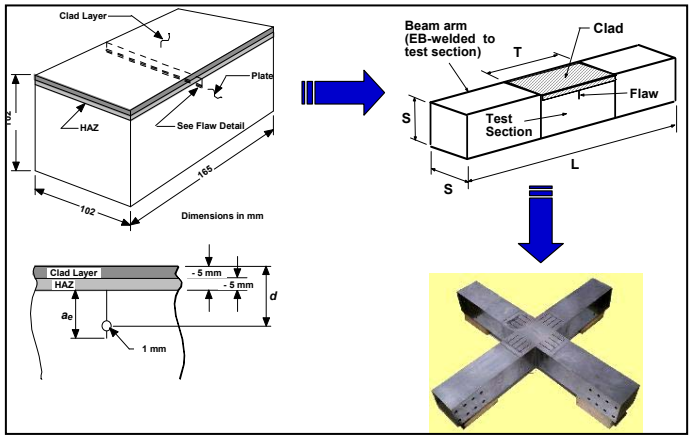


**Fig. 1: Design of uniaxial bend beam component, using a through-slot to simulate an embedded flaw**

The embedded-crack specimens were tested in the following order: Unclad 4 1.1, Unclad 4 1.2, Clad 4 2.2, and Clad 4 2.1, with test temperatures of -128 °C, -95 °C, -75 °C and -95 °C respectively.

The photograph in Fig. 2 shows the exposed fracture surface and the initial fatigue-sharpened embedded flaw of the test Unclad 4.1.1.

**Fig. 2: Test 4.1.1 (Unclad): T = -128 ˚C: fracture surface after test**

The longitudinal moment versus crack mouth opening displacement (CMOD) data of the four tests are compared in Fig. 3. There is no significant difference in the global behavior of both beam types obvious. The cladded beams are slightly weaker in the elastic regime.

Because from the experimental results no information was obtained which crack front failed first, an impotant objective of the subsequent analyses should be to give the probability of failure for each of the crack fronts.

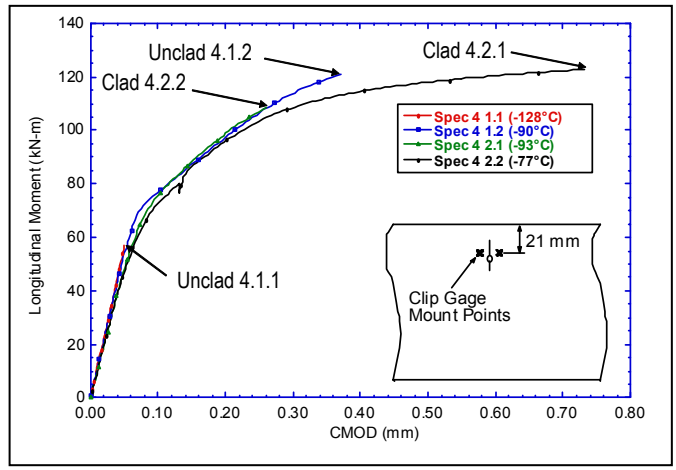


**Fig. 3: Comparison of load-deflection curves of the tests (unclad and clad)**

## Surface cracks

For the surface crack testing six clad cruciform specimens were fabricated by ORNL. The specimen design is termed "intermediate-scale," measuring 102 mm in thickness. Four load-diffusion control slots are included in each side of the test section to provide lateral flexibility in the interface between test section and beam arm. A shaped electrode was used to machine a three-dimensional (semi-elliptic) through-surface flaw in the test section. The length orientation of the flaw is parallel to the longitudinal weld. The flaw depth extends in the weld through-thickness direction. The specimens are fatigue pre-cracked in the longitudinal beam configuration. During fatigue pre-cracking, the flaw was extended an additional 1.3 mm along its full length. The final nominal dimensions are 53.3 mm long and 19.1 mm deep. The transverse beam arms are then electron-beam welded onto the longitudinal beam, giving the completed clad cruciform specimen as shown in Fig. 4.

All six specimens were tested to failure under fully 1:1 biaxial loading. Measured longitudinal moment versus CMOD, as recorded by the Data Acquisition System (DAS) for the specimens PVR-3, PVR-5, PVR-6, PVR-2 and PVR-1, are depicted in Fig. 5; the data are presented in the order in which the specimens were tested.

The key experimental variable is the target test temperature of the beam. Ideally the full series of cruciform beams would be tested at a single temperature to facilitate statistical analysis of the results. However selection of a suitable temperature is not straightforward, a point perhaps indicative of the current level of reliability of transferability methods from standard fracture test methods to more complex loading situations. The objective was to achieve cleavage failure of the cruciform specimen in the non-linear region of the load-versus-CMOD curve. This approach was used successfully in previous HSST testing programs to quantify the effects of biaxial loading on crack-tip constraint.

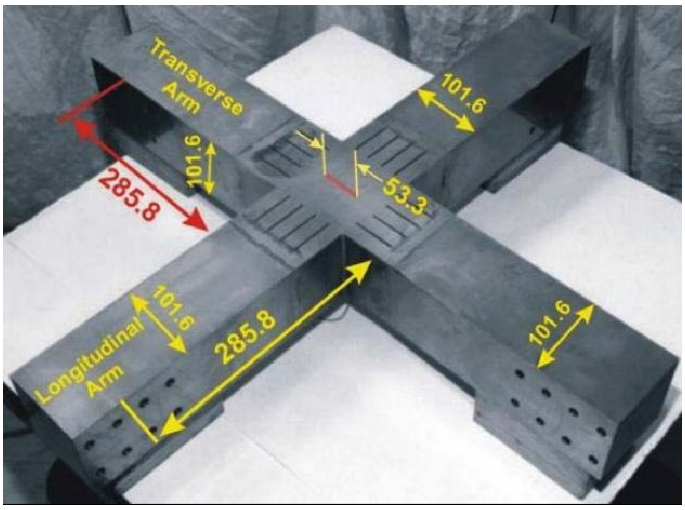


**Fig. 4: Tests on clad cruciform specimens with a surface flaw**

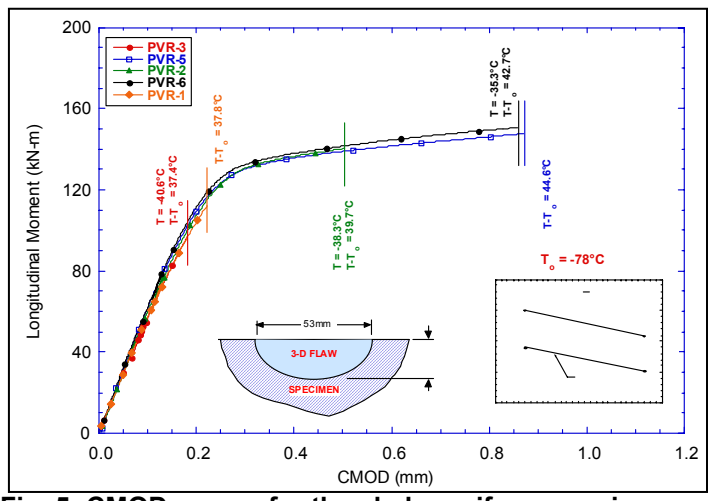


**Fig. 5: CMOD curves for the clad cruciform specimen tests**

## NUMERICAL INVESTIGATIONS

The analytical approach for cleavage fracture assessment applied by ORNL and Framatome is based on a Weibull stress statistical fracture model, where the parameters for the model are estimated using the G-R-D calibration scheme [3] developed at the University of Illinois. In the ORNL calculation of the Weibull stress the hydrostatic stress as the effective stress is used in order to capture the constraint effect due to both shallow flaw effects and biaxial, in the Framatome model the principal stresses are used.

The Weibull stress calibration was conducted with the following features using finite-element models of SE(B) specimens:

Given the estimated reference temperature To values and high-constraint conditions with a 1T flaw length, fracture toughness KJc (or Jc) data were stochastically-simulated from the Master-Curve Weibull statistical model. A sample size between 50 and 60 was chosen in the calculation, where calibration convergence for this sample size was demonstrated in a previous study.

Using the simulated 1T *Jc* data set (converted from $K_{Jc}$), an iterative Weibull stress calibration was carried out using 1T SE(B) bend-bar finite-element models ($a/W$ = 0.1 for low constraint and $a/W$ = 0.5 for high constraint) at temperature –100 °C.

The Weibull stress *shape parameter* ($m$), obtained from this calibration procedure, is assumed to be temperature invariant as discussed in [4].

A modified Weibull stress calibration approach was recently developed at ORNL and Framatome to calculate the reference temperature $T_0$ at different constraint levels using the following procedure:

(a) With the calibrated value for $m$ using the SE(B) finite-element models, map the stochastically-generated data (both shallow-flaw and deep-flaw datasets) from the SE(B) shallow-flaw ($J_{low}$) and deep-flaw ($J_{high}$) Weibull stress $\sigma_W$ vs. $J_C$ curves back to the SSY curve ($J_{ssy}$). The four fracture toughness data sets ($J_{low}$, $J_{high}$, $J_{low\text{-}SSY}$ and $J_{high\text{-}SSY}$) represent three constraint levels: (1) *low constraint*, (2) *high constraint*, and (3) *SSY constraint* (combined $J_{low\text{-}SSY}$ and $J_{high\text{-}SSY}$).

(b) Convert the mapped *Jc* data to *KJc* by the plane-strain conversion.

(c) Calculate the corresponding $T_0$ values for each dataset based on the procedure in ASTM E-1921 [5].

### Embedded cracks

The analyses of the embedded cracks loaded by uniaxial bending were performed by ORNL and Framatome. Both partners used the general purpose finite element code ABAQUS [6] for the fracture mechanics investigations. The Weibull stresses were calculated by own post processor codes.

The outcome of the numerical analysis is compared to the experimental values. By means of the Weibull calibration model the probability of failure is predicted in respect of:

- Which crack front is most likely to fail first?
- Is there a difference in the failure behavior between the cladded and uncladded specimen?
- Is there a constraint caused shift in the transition temperature $T_0$ compared to regular fracture toughness specimens?

### Global results

The comparison of the global results load-deflection is shown in Fig. 6. Two of the four tests at the same temperature are compared to the numerical outcome: clad test 4.2.1 carried out at T = -93°C and unclad test 4.1.2 carried out at T = -90°C. In the numerical analysis all material data are scaled to a temperature of -90°C. It can be seen that the global behavior of both specimens is very similar. The uncladded specimen is slightly stiffer in the elastic regime, but overall all curves lie

together within a small scatterband and the agreement between experiment and calculation is very good.

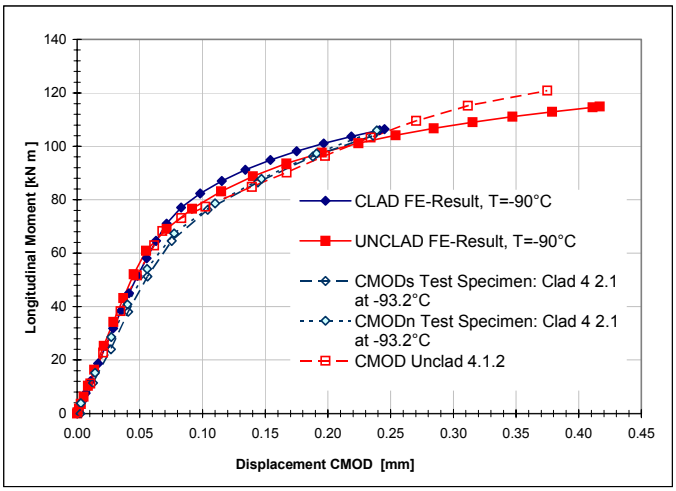


**Fig. 6: Load vs. CMOD history for uncladded and cladded NESC specimen and FE-Results at -90°C for both specimens**

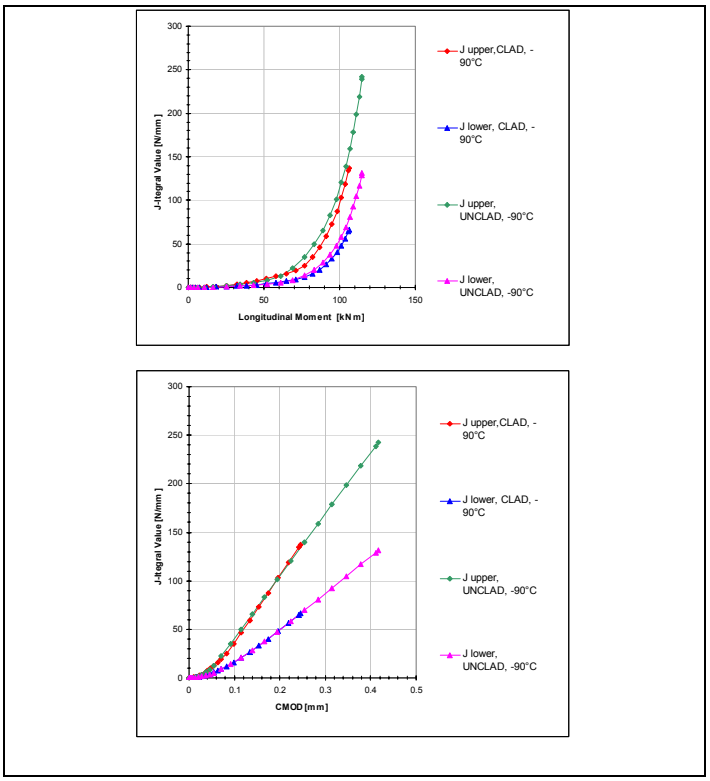


**Fig. 7 J-Integral vs. longitudinal moment and CMOD for cladded and uncladded NESC specimen at -90°C**

The calculated J-Integral is given in Fig. 7. In each diagram the upper and the lower crack fronts are differentiated as well as the cladded and uncladded specimens. The upper crack front is the one nearer to the inner or the clad surface. This one is generally higher loaded due to the stress distribution of the applied bending moment; therefore also the J-Integral values are higher at this crack front, as can be seen in Fig. 7, where it is plotted against the applied moment and the crack mouth opening displacement (CMOD). There is only a slight difference in J-Integral between the cladded and uncladded specimens versus moment and no difference, if both specimens are compared with respect to CMOD.

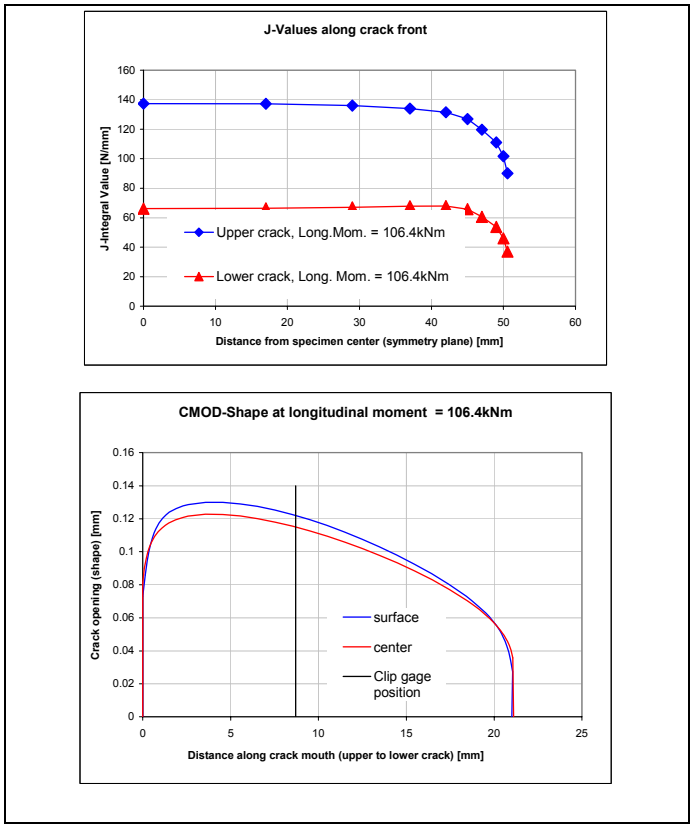


**Fig. 8: J-values along both crack fronts at failure moment. CMOD-shape at the same loading state in the center and at the surface**

In Fig. 8 the variation of J-Integral of the cladded specimen with respect to crack front position is shown. J is constant along the crack front up to high loads and it varies only at the free surfaces. In addition shape of the crack mouth opening at failure moment is shown. The upper crack front is obviously more opened due to the higher bending stresses.

## Local results

The following section describes the calibration and application of the statistical Weibull model. It should be used to analyze the failure mechanism of the beam and to predict the constraint based shift in transition temperature $T_0$.

The ORNL analytical approach for cleavage fracture assessment is based on a Weibull stress statistical fracture model, where the parameters for the model are estimated using the G-R-D calibration scheme [3] developed at the University of Illinois. The calculation of the Weibull stress uses the

hydrostatic stress as the effective stress in order to capture the constraint effect due to both shallow flaw effects and biaxial.

The Weibull stress shape parameter (m), obtained from this calibration procedure, is assumed to be temperature invariant as discussed in [4]. The results of the calibration are shown in Fig. 9 where the calibrated Weibull shape parameter m = 3.4.

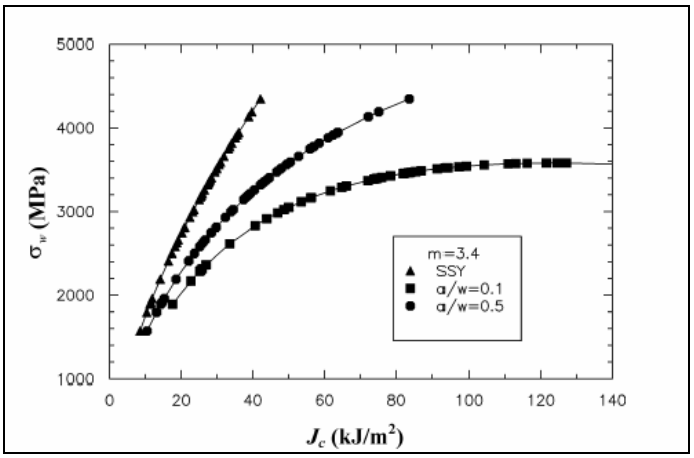


**Fig. 9: Weibull stress as a function of *J*-integral for the converged calibration: *T* = -100 °C, *m* = 3.4, Plate 100 material, 50 stochastically-generated SE(B) fracture toughness data points**

After the Weibull model has been calibrated by means of the SE(B) specimens, the Weibull stresses for the uniaxial loaded beams are calculated with the obtained m-parameter. The finite element model used by ORNL is shown in Fig. 10. The sharp-tip model has a small root radius of 0.001 mm, and contains 35,303 nodes and 7,580 elements. It was used to precisely calculate the through-thickness (average) fracture toughness $J_{applied}$ for both the top and bottom crack tips.

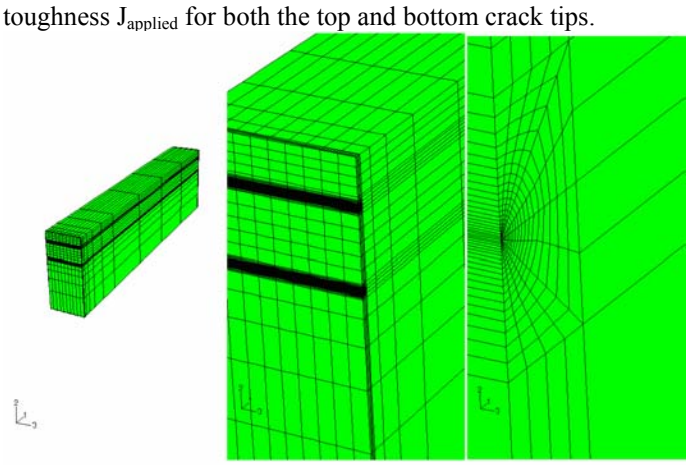

**Fig. 10: Finite element 1/4 model of 4T beam specimen containing embedded sharp-tip flaw**

The blunt-tip model (with a finite root radius of 0.0254 mm) was built with 39,353 nodes and 8,440 elements as shown in Fig. 11. This blunt-tip model was used to calculate the stress and displacement fields for the Weibull stress calculation (with Weibull shape parameter m = 3.4) with a modified WSTRESS (Version 2.0) [8] code. Very detailed finite element analyses were conducted on the embedded-flaw beam models with material properties based on a temperature of –100 °C (close to the bending test temperatures).

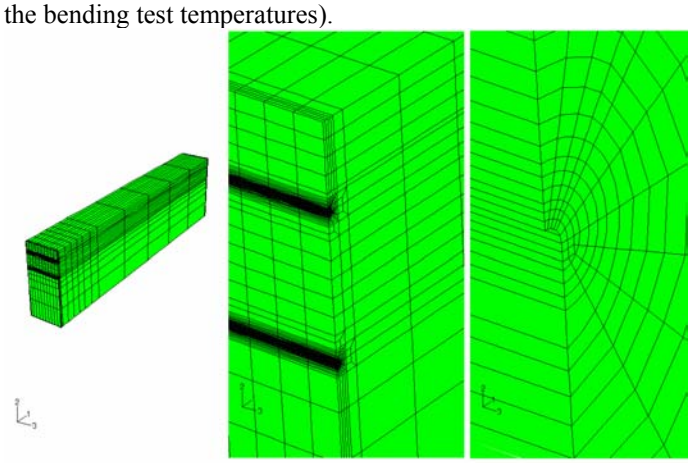

**Fig. 11: Finite element 1/4 model of 4T beam specimen containing embedded blunt-tip flaws**

Fig. 12 shows the Weibull stresses ($\sigma_w$) of the ORNL anlyses of the cladded beam for the top and bottom crack tips as a function of applied longitudinal bending moment. Fig. 12 indicates that the top-crack-tip Weibull stresses $\sigma_w$ are greater than bottom-crack-tip Weibull stresses. This result is due to the fact that the top crack tip is farther away from the neutral axis of the beam during bending and is, therefore, subjected to a higher applied stress than the bottom crack tip. The top crack tip driving force, Japplied, is also greater than the bottom crack tip driving force.

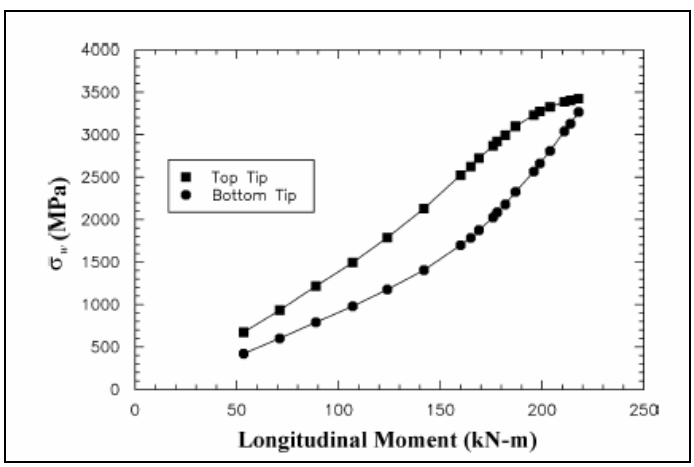


**Fig. 12: Weibull stress load path for top and bottom crack tips as a function of applied bending moment (ORNL)**

On the other hand, this model also captures the constraint effect due to the different location of the crack, as shown in Fig. 13. As expected, the bottom-tip has higher constraint, and the Weibull stresses there are larger with the same fracture toughness value.

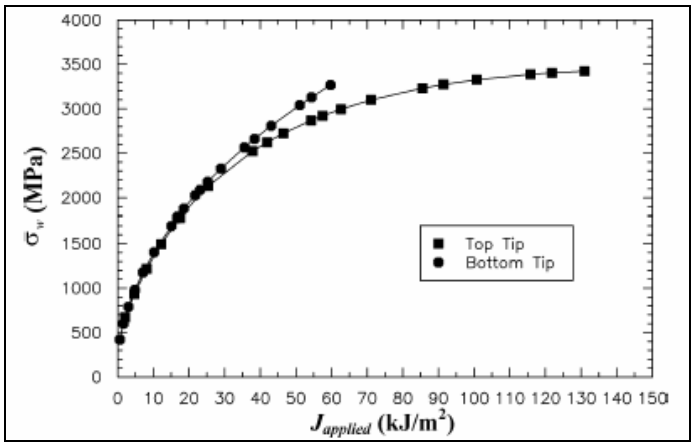


**Fig. 13: Weibull stresses at the top and bottom crack tips as a function of applied driving force (ORNL)**

A comparison between uncladded and cladded beams can be made by the Framatome analyses, Fig. 14. In both cases the higher constraint is like in the ORNL analysis at the bottom-tip (lower crack) this means a loss of constraint for the top-tip (upper crack). The cladded specimens show a loss of constraint for both crack fronts compared to the uncladded specimen.

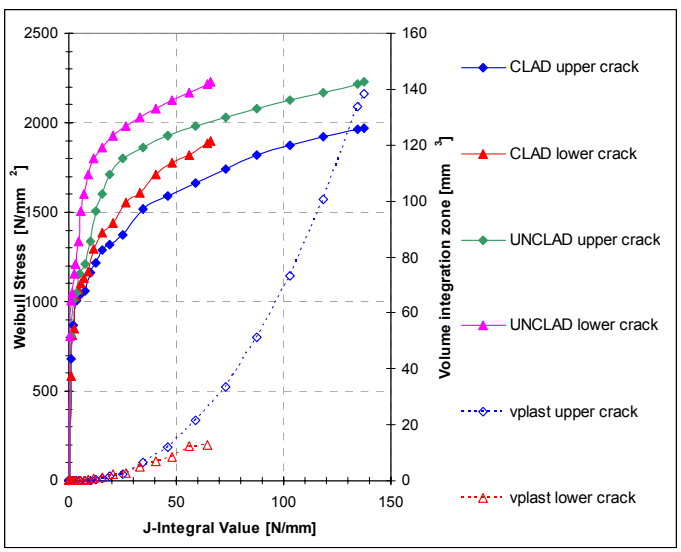


**Fig. 14: Comparison of Weibull stress vs. J for cladded and uncladded specimens (Framatome)**

An important objective of this analysis is to produce estimates of the probabilities of cleavage initiation for both flaw tips. Therefore, it is necessary to calculate the cumulative failure probability (Pf) of the top and bottom crack tips. In order to decide which tip fails first during the bending, it is better to compare $P_f$ under the same bending moment instead of same J-Integral. The $J_c$ dataset in the $P_f$ Vs. $J_c$ is converted to corresponding longitudinal moment values using polynomial approximation of $J_{applied}$ Vs. bending moment. Figure 15 shows $P_f$ at top and bottom tips as a function of longitudinal bending moment. It is clear to see that the top-tip fails first during bending, even though the bottom-tip has higher level of constraint.

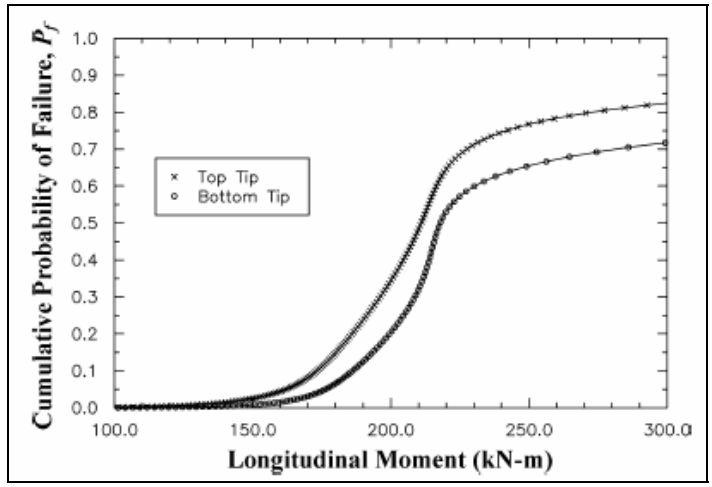


**Fig. 15: Cumulative failure probabilities for the top and bottom crack tips as a function of applied bending moment (ORNL)**

In Fig. 16 the probability of failure is given for the Framatome analyses of the two investigated beams (cladded and uncladded) versus the applied moment. As already seen from the Weibull plots, the top-tip (upper crack) of the cladded specimen is more likely to fail prior to the bottom-tip (lower crack), not due to higher crack front constraint, but only due to higher J-Integral values at same bending moment.

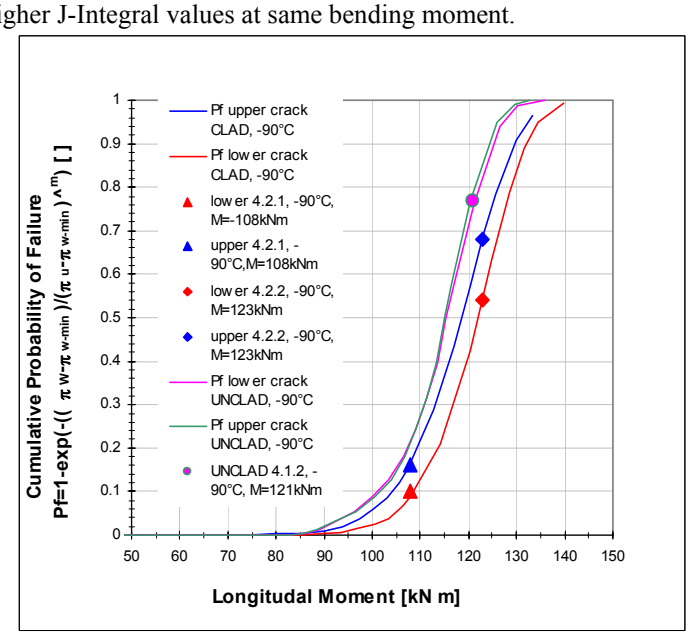


**Fig. 16: Cumulative probability of failure vs. longitudinal moment & CMOD for cladded and uncladded beam at T=-90°C (Framatome**

The two performed tests which are calculated at T = -90°C, but which are conducted at T = -93°C (4.2.1) and T = -77°C

(4.2.2) give reasonable failure probabilities at the experimental failure moments.

The probability versus moment shows that the uncladded beam fails at lower moments than the cladded beam, but both crack fronts at the same time. The cladded beam fails later and the top-tip (upper crack) slightly earlier than the bottom-tip (lower crack).

If the failure probability is plotted versus the CMOD, all specimens and crack fronts fail practically at the same CMOD.

## Surface cracks

The investigations of the surface cracks are carried out by ORNL. For the calibration fracture toughness data of SE(B) 1T specimens tested at T=-100°C are used and data sets at the test temperature of the large scale beams T=-40°C are simulated using the transition temperature and the Master Curve, see Fig. 17. The deep crack model had a transition temperature of $T_0$ = -88.3°C and the shallow crack model a $T_0$ = -132.8°C. The finite element calculations are performed with the commercial code ABAQUS [6]. Two different models for each specimen type are constructed: the sharp crack tip models are used to calculate the global behaviour and the J-Integral, the outcome of blunt crack tip models are used for the calculation of the Weibull stresses. The FE models with the blunt-tip for the calibration together with the von Mises stresses are shown in Fig. 18 and Fig. 19.

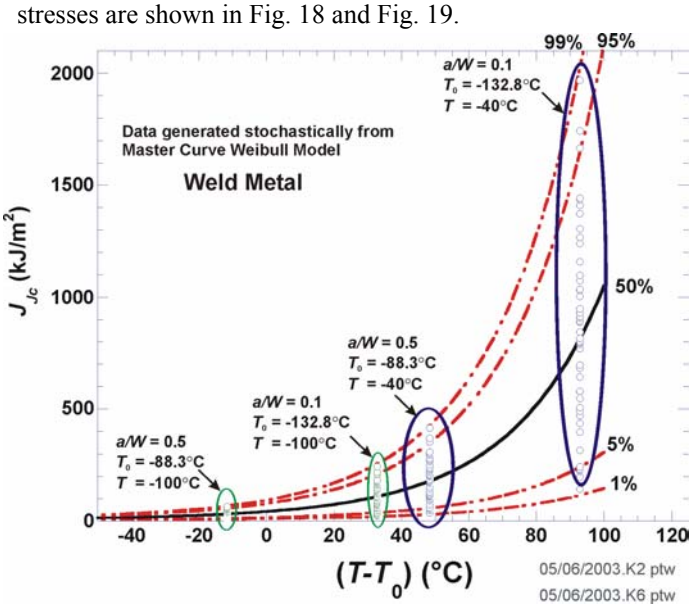


**Fig. 17: Weld metal fracture toughness data used for the calibration**

The calibration of the Weibull stress model parameters was carried out using the G-R-D calibration scheme. The calculation is based on the hydrostatic stress to capture the constraint effects due to both the shallow crack and the biaxial loading effect. A Weibull shape parameter of m= 6.35 was obtained. The results of Weibull stress versus J-Integral of the shallow and deep crack SE (B) 1T specimens is shown in Fig. 20.

After the Weibull stress model was calibrated, the large scale beams analyses were carried out. The according finite element mesh is given in Fig. 21. The semi-elliptical surface crack is located in the weld of the cladded insert and loaded by biaxial load. The a/W ratio of the deepest point of the crack has a value of 0.1.

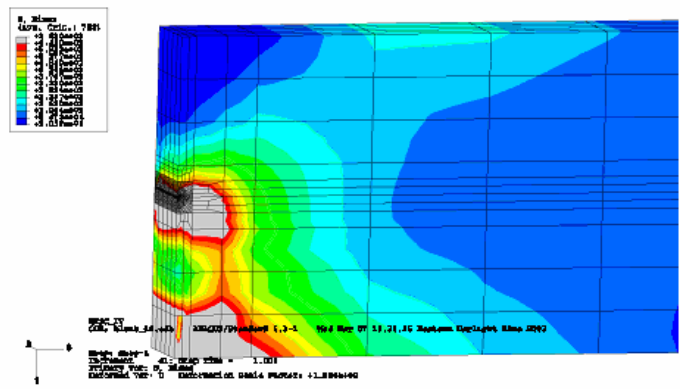

**Fig. 18 Deformed blunt tip of the deep crack SE(B) specimen**

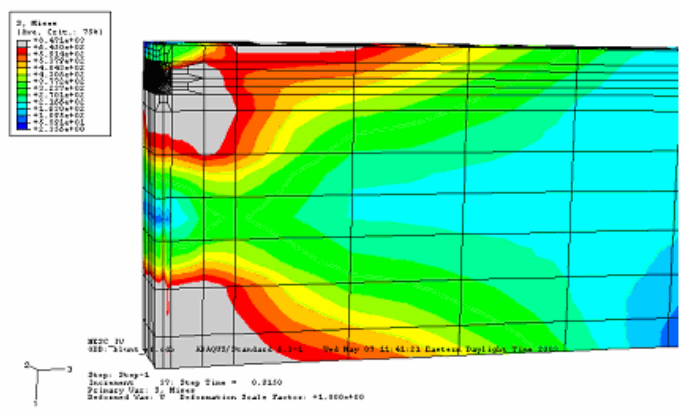

**Fig. 19 Deformed blunt tip of the shallow crack SE(B) specimen**

The objective of this analysis is to predict the probability of cleavage initiation by means of the calibrated three-parameter Weibull stress model:

$$P_f(\sigma_w) = 1 - \exp[-(\frac{\sigma_w - \sigma_{\min}}{\sigma_u - \sigma_{\min}})^m],$$

$$P_f \sim J_{IC}$$

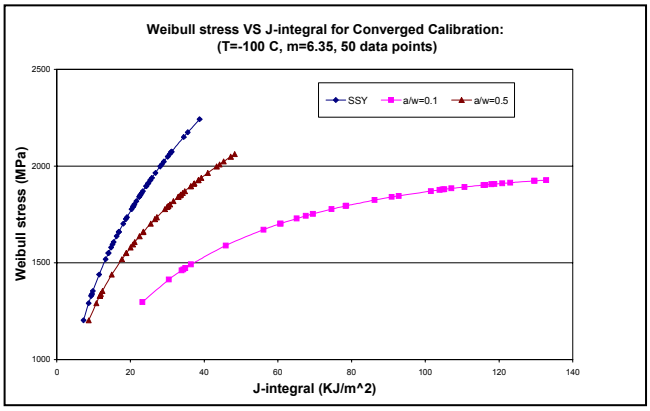


**Fig. 20 Calibration of the Weibull stress parameters**

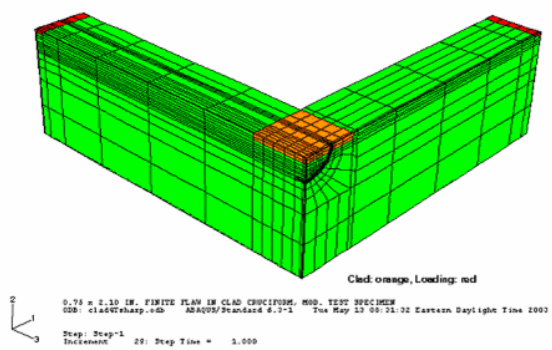


**Fig. 21 Finite element ¼ model of cruciform 4T beam specimen containing semi-elliptical surface crack (*a/w* = 0.1)**

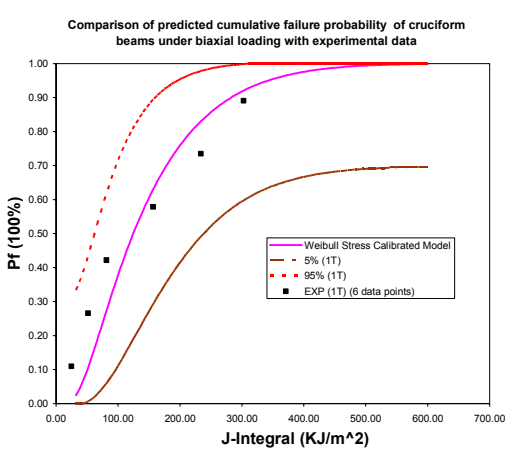


**Fig. 22 Cumulative failure probability of cruciform beams under biaxial Loading; comparison of prediction and experiment**

Six test results of the cruciform beams tested to failure are compared with the numerical outcome in Fig. 22. The cumulative failure probability of the cruciform beams is predicted. For comparison with the experiments, a median-rank order statistics of the experimental data is used. The prediction lies within 90% confidence limits of the experimental data.

## CONCLUSION

The analyses of the NESC IV experiments by means of recently developed advanced fracture mechanics methods using the Weibull stress model to predict the failure of large scale beams show that surface as well as embedded crack effects could be well taken into account. The consideration of constraint effects of the investigated shallow cracks under uniaxial as well as biaxial loading could be described and verified by the experimental outcome. The application of these advanced models to a variety of different geometries and loading conditions encourages for the general use in structural assessments.

## REFERENCES


[1] B. R. Bass et al, NESC-IV Project – An Investigation of the Transferability of Master Curve technology to shallow flaws in reactor pressure vessel appliactions, Interim Report NESCDOC MAN (02) 04, June 2002

[2] B. R. Bass and W. J. McAfee, "NESC IV project Phase I: Fracture tests of shallow cracks in biaxially-loaded cruciform beams extracted from the inner surface of an RPV (Quick-Look Report)", NESC DOC MAN(01) 06, September 2001

[3] X. Gao, C. Ruggieri, and R. H. Dodds, Jr., "Calibration of Weibull Stress Parameters using Fracture Toughness Data," *International Journal of Fracture* 92, (1998) 175-200.

[4] J. P. Petti and R. H. Dodds, "Calibration of the Weibull Stress Scale Parameter, $_u$ $\sigma$, Using the Master Curve," submitted to *Engineering Fracture Mechanics*, 2003.

[5] "Standard Test Method for Determination of Reference Temperature, $T_0$, for Ferritic Steels in the Transition Range," E 1921-97, Annual Book of ASTM Standards Section 3: Metals Test Methods and Analytical Procedures, Vol. 03.01 *Metals – Mechanical Testing; Elevated and Low-Temperature Tests; Metallography*, American Society for Testing and Materials, West Conshohocken, PA, 1998.

[6] *ABAQUS/CAE User's Manual, v. 6.3*, Hibbitt, Karlsson, and Sorensen, Inc., Pawtucket, RI, 2002.

[7] N. Taylor, B. R. Bass, "Overview of NESC IV cruciform specimen test results", Proceedings of the ASME PVP Conference, August 2002, Vancouver, Canada

[8] Ruggieri, C. and Dodds, Jr., R. H., "Numerical Evaluation of Probabilistic Fracture Parameters with WSTRESS," *Engineering and Computers*, Vol. 15, No. 1, 1998, pp. 49-73